Supplementary Information (SI) for Energy & Environmental Science.
This journal is © The Royal Society of Chemistry 2026

Supplementary Information:

Replicability challenges in redox flow cell testing: Insights from a multi-institutional study

Hugh O'Connor[1,†], Alexander H. Quinn[2,†], Edward Saunders[3,4], Aodhán Dugan[1], Thomas Goodwin[2], Nadia Farag[3], Greta Thompson[3,4], Ameya Bondre[5], Marina Tabuyo-Martinez[5], Hannah M. Burnett[6,7], Thomas Y. George[7], Jordan D. Sosa[8], Carlos Mingoes[9], Peter Nockemann[1], Clare P. Grey[3], Dominic Wright[3], Michaël De Volder[4], Antoni Forner-Cuenca[5], Robert A. W. Dryfe[6,7], Michael J. Aziz[8], Ana B. Jorge Sobrido[9], Fikile R. Brushett[2], Josh J. Bailey[1,*]

[†] Co-first author
* Corresponding author: j.bailey@qub.ac.uk

[1] School of Chemistry and Chemical Engineering, Queen's University Belfast, Belfast BT9 5AG, United Kingdom
[2] Department of Chemical Engineering, Massachusetts Institute of Technology, Cambridge, Massachusetts 02139, United States of America
[3] Yusuf Hamied Department of Chemistry, University of Cambridge, Cambridge CB2 1EW, United Kingdom
[4] Department of Engineering, University of Cambridge, Cambridge CB3 0FS, United Kingdom
[5] Department of Chemical Engineering and Chemistry, Eindhoven University of Technology, 5600 MB Eindhoven, The Netherlands
[6] Department of Chemistry, University of Manchester, Oxford Rd, Manchester M13 9PL, United Kingdom
[7] Henry Royce Institute, University of Manchester, Oxford Rd, Manchester M13 9PL, United Kingdom
[8] Harvard John A. Paulson School of Engineering and Applied Sciences, Cambridge, Massachusetts 02138, United States of America
[9] School of Engineering and Materials Science, Queen Mary University of London, London E1 4NS, United Kingdom

Table of contents

Section S1: Additional materials and methods

Round robin design

Here we include some details collected from the surveys which may be of interest but are not necessary for interpreting the main manuscript. With regards to experience, the positions of participants ranged from a few months into their doctoral studies to postdoctoral research associates. Participants spanned the fields of Chemical Engineering, Chemistry, and Materials Sciences & Mechanical Engineering, with *ca.* 70% working with flow cells daily or weekly, and *ca.* 30% working with them monthly. Experience to date with flow cells was estimated to range from novices (no experience) to those with 1000+ h. Motivations for participation varied, including: (all paraphrased) to develop and share best practices; improve interlaboratory comparisons of flow batteries; highlight rarely reported features of flow battery assembly and operation; learn new protocols; and develop collaborations in this field. The pre-experiment survey also highlighted the range of flow battery chemistries investigated by the participants including, but not limited to: iron chloride; iron coordination complexes; vanadium; and organic molecules in acidic, neutral, and basic aqueous electrolytes, as well as organic molecules in nonaqueous electrolytes. Participants had experience working with an array of flow cells, ranging from in-house builds to commercial offerings. Membrane preferences were spread across Nafion® membranes (of various types), in-house fabricated membranes (*e.g.*, sulfonated poly(ether ether ketone)), and Fumasep® membranes (again, of various types). Similarly, electrode preferences were spread across graphite and carbon felts, papers, and cloths with variable pre-treatment methods being routinely employed. Data analysis procedures differed in software use, including processing data with potentiostat manufacturer software (*e.g.*, EC-lab, Gamry Echem Analyst, NOVA), scripting (Python, MATLAB), and use of Microsoft Excel or OriginLab Origin. Distinctions in experimental practices included the use or omission of gas sparging, the choice of sparging gas (argon or nitrogen), the use or omission of sparging gas pre-humidification, as well as stirring of reservoirs (or lack thereof), flow-cell componentry cleaning practices, and electrical configurations for connecting the cell to the potentiostat.

Flow cell test kits

The flow cell used in this study was based on a 3D-printed, "flow-through" design developed by some of the authors in previous work.[37] It included flow frames fabricated from acrylonitrile butadiene styrene (ABS) filament (Ultimaker, Netherlands) using an Ultimaker S5 3D-printer, featuring simple diffuser-style manifolds and a fixed cavity thickness. The individual components of the test kit are shown in **Figure S1 a**, with a detailed view of a 3D-printed half-cell in **Figure S1 b**. **Figure S1 c** and **d** show 3D renders of the fully assembled cell and a corresponding exploded view of its components, respectively Initial test kits distributed featured integrated plastic connectors that proved robust under normal laboratory use; however, all units shipped were found to be damaged upon arrival, likely due to mechanical stresses incurred during transit. As a result, a re-designed version of the flow cell was distributed (**Figure S1b**) and used exclusively for all experimental data presented here. The updated design incorporated threaded polypropylene hose barbs, which were pre-installed in the 3D-printed parts and sealed using Loctite 55 thread sealing cord (Henkl Ltd., Germany) prior to distribution. Another key modification from the previously-published designs was the use of aluminium end plates, fastened around the perimeter with eight M6 bolts to ensure uniform compression across the cell.[16,37] To facilitate parametric editing, files are supplied in the native formats of SolidWorks (.sldprt) and Fusion360 (.f3d). For wider compatibility, the components are also available in exchange formats (.stl and .step). Additionally, the cell body has been re-created in FreeCAD (.FCStd), and .dxf files required for laser-cutting the gaskets are included. To ensure that participants could reliably assemble the cells, detailed instructions and a pictorial assembly guide were included with each kit.

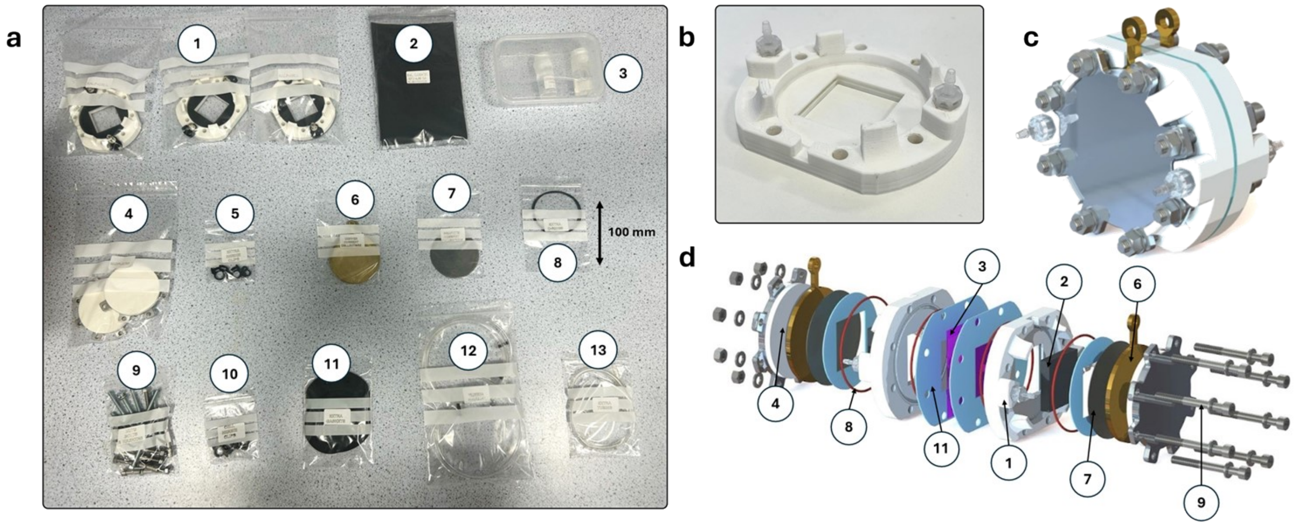

Figure S1. (a) Photograph showing contents of test kits distributed to study participants: 1) 3D-printed flow frames, 2) graphite felt electrode material, 3) membrane in deionised water, 4) end plates, 5) tubing clips, 6) brass current collectors, 7) graphite-polymer composite current collectors, 8) O-rings, 9) nuts, bolts, and washers, 10) additional clips, 11) gaskets, 12) peristaltic pump and transfer tubing, and 13) additional tubing. (b) A photograph of the 3D-printed half-cell body used in the study. (c) A render of the fully assembled flow cell. (d) An exploded view of flow cell with key components labelled as shown in (a).

Table S1. Bill of materials for study cell-testing kit including component quantities and descriptions, supplier/catalogue numbers, and estimated costs (USD) on a *per* kit basis.

Component	**Quantity**	**Description**	**Supplier/Catalogue number**	**Material cost ($/kit)**
Flow frames	4	3D-printed from Ultimaker ABS white filament. 16 cm^2 active area (9 per 750 g filament reel)	RS Components/ 134-8171	28.26
Polypropylene tube connectors	6	Male Thread: 1/8" NPT –Tube ID: 1/8"	Christy Hydraulics/ cXN4S4	10.17
Brass current collectors	2	Grade CZ108 brass – 300 × 200 × 4 mm^3 (8 per sheet with off-cuts)	Ringwood metal	16.50
Graphite-polymer composite current collectors	2	SGL Carbon SIGRACELL® PV15 960 × 640 × 0.6 mm^3 sheets (96 per sheet with off-cuts)	SGL Carbon	3.88
Aluminium end plates	2	Machined from 4” Aluminium Round Bar Alloy 6082 T6	AALCO Metals	3.87
Isolation plates	2	3D-printed from Ultimaker ABS white filament. 16 cm^2 active area (25 per 750 g filament reel)	RS Components/ 134-8171	3.02
Socket head bolts	12	M6 × 60 mm Hex Socket Cap Screw Plain Stainless Steel	RS Components/ 293-410	16.96
Hex bolts	12	Bright zinc-plated steel hex bolts M6 × 60 mm	Screwfix/ 14709	2.79
Nuts	14	A2 stainless steel hex nuts M6	Screwfix/ 6386T	1.63
Washers	28	A2 stainless steel flat washers M6 × 1.6 mm	Screwfix/ 7614T	1.04
Gaskets	24	1.5 mm thick EPDM sponge, 225 cm^2 per half-cell accounting for off-cuts	PAR-Direct/ ENSP-1m-1.5	6.53
O-rings	9	Nitrile O-rings, 70 ShA, 70 mm ID × 1.78 mm CS	Polymax/ 70X1.78N70	4.89
Electrodes	3	SGL Carbon 4.65 EA, 3 pieces of ca. 20 × 15 cm^2	SGL Carbon	1.44
Tubing clips	4	5.4-6.3 mm diameter Herbie Clip Plastic Hose Clip 4.2 mm band in Black Nylon	Westfield Fasteners	1.23
Peristaltic pump tubing	2	Saint Gobain Tygon® E-3603 PVC clear flexible tubing, 3.2 mm ID, 6.4 mm OD, 2× 150 mm lengths	RS Components/ 313-9505	0.24
Thread sealing cord	2	Loctite 55 thread sealing cord, 2x 15 cm lengths (one length per nozzle)	RS Components/ 280-5020	0.06
Rigid FEP tubing	4	Nalgene™ 890 FEP Tubing 1/16” ID, 1/8” OD ca. 50 cm	ThermoFisher Scientific/8050-0125PK	3.67
Membrane	2	Solvay Aquivion® E98-15S membrane ca. 8 × 8 cm^2 (cost accounting for unusable off-cuts from 60 × 250 cm^2 roll)	Fuel Cell Store	31.14

Total	137.32

3D-printed flow frame design and post-processing

The cell components were designed using SolidWorks 2023 Research Edition (Dassault Systèmes SE, France). CAD files were exported as .STL files and imported into Ultimaker Cura 4.11.0 (Ultimaker, Netherlands) for slicing. The authors note the importance of using the specific version of the slicing software as default printing parameters may vary in future Cura versions. Each flow frame design consisted of two .STL files, one for the main body and one for the O-ring channel, which were aligned and printed together as a single component. Default material settings were applied, except where noted in Table S4. These print parameters were refined from a previous publication by some of the authors to reduce porosity and eliminate surface seams that could act as electrolyte leak paths.[1]

Table S2. Changes from default 3D-printing settings.

Parameter	**Default**	**Custom**
Material flow	100%	115%
Initial layer material flow	100%	115%
Z-alignment seam	Sharpest corner	Random
Randomise infill start	Checked	Unchecked
Build plate adhesion	Checked	Unchecked
Support placement	Touching build plate	Everywhere

To ensure that the surface quality of the O-ring channel was adequate for sealing, different print settings were applied in this region. Due to effects of “bridging”, exacerbated by the increased material flow rate, certain areas of the unsupported O-ring channel had poor print quality. To mitigate this, the “*per* model settings” feature within Ultimaker Cura was used to apply 100% material flow rate and a print speed of 30 mm s^{-1} solely to this part. “Supports” were only used within the manifold section (excluding the inlet and outlet sections), with support blockers positioned elsewhere. These changes to default settings are reflected in the .3MF and .GCODE files provided. Two half-cells were printed simultaneously on each build plate, with a total print time of *ca.* 19 h.

The flow frames were fabricated using Ultimaker ABS White 3D-printing filament (Ultimaker, Netherlands) on an Ultimaker S5 3D printer equipped with a 0.4-mm diameter nozzle. Printing was performed on a glass build plate coated with Dimafix adhesive (DIMA 3D, Spain) to ensure adequate adhesion during printing and to facilitate removal after the build plate had cooled. Following removal from the build plate, the 3-mm inlet and outlet ports were widened using a pillar drill and an 8.7-mm drill bit to a depth of 15 mm. Threads were then manually cut using an NPT 1/8" × 27 tap bit (Avon Engineering, United Kingdom). Polypropylene tubing connectors with a male 1/8" NPT thread and 1/8" hose barb (Christy Hydraulics, UK) were installed and sealed using *ca.* 20 cm of Loctite 55 Pipe Sealing Cord (Henkel Adhesives, Germany).

Manufacture of non-3D-printed components

Endplates were CNC-machined from Aluminium Round Bar Alloy 6082 T6 (AALCO, United Kingdom). ABS isolation plates were 3D-printed and bonded to the aluminium endplates using Loctite Precision Super Glue (Henkel, Germany). Several participants reported detachment of the isolation plates from the endplates during transit. In subsequent in-house testing, the bonding method was changed to a two-part epoxy adhesive (Araldite 2014, Huntsman Corporation, USA) and was found to provide improved adhesion. The current collectors comprised two waterjet-cut components: Grade CZ108 brass (Ringwood Metal, UK), which interfaced with the external testing equipment, and SIGRACELL® PV15 (SGL Carbon, Germany), which was used to prevent corrosion of the brass during electrochemical testing. All machining operations were performed in the School of Mechanical and Aerospace Engineering workshop at Queen’s University Belfast (QUB). Engineering drawings of these components are provided in **Figure S2 a-c**.

Expanded EPDM gaskets (1.5-mm thickness; PAR Group, United Kingdom) were laser-cut using a 25 W CO_2 desktop laser cutter (HPC LS3040, HPC Laser, UK). LightBurn software (LightBurn, USA) was used to control the laser cutter and define the cutting parameters. CAD designs were exported from SolidWorks as .DXF files and imported into LightBurn. The laser was operated at 60% power (*ca.* 15 W) with a cutting speed of 50 mm s^{-1}.

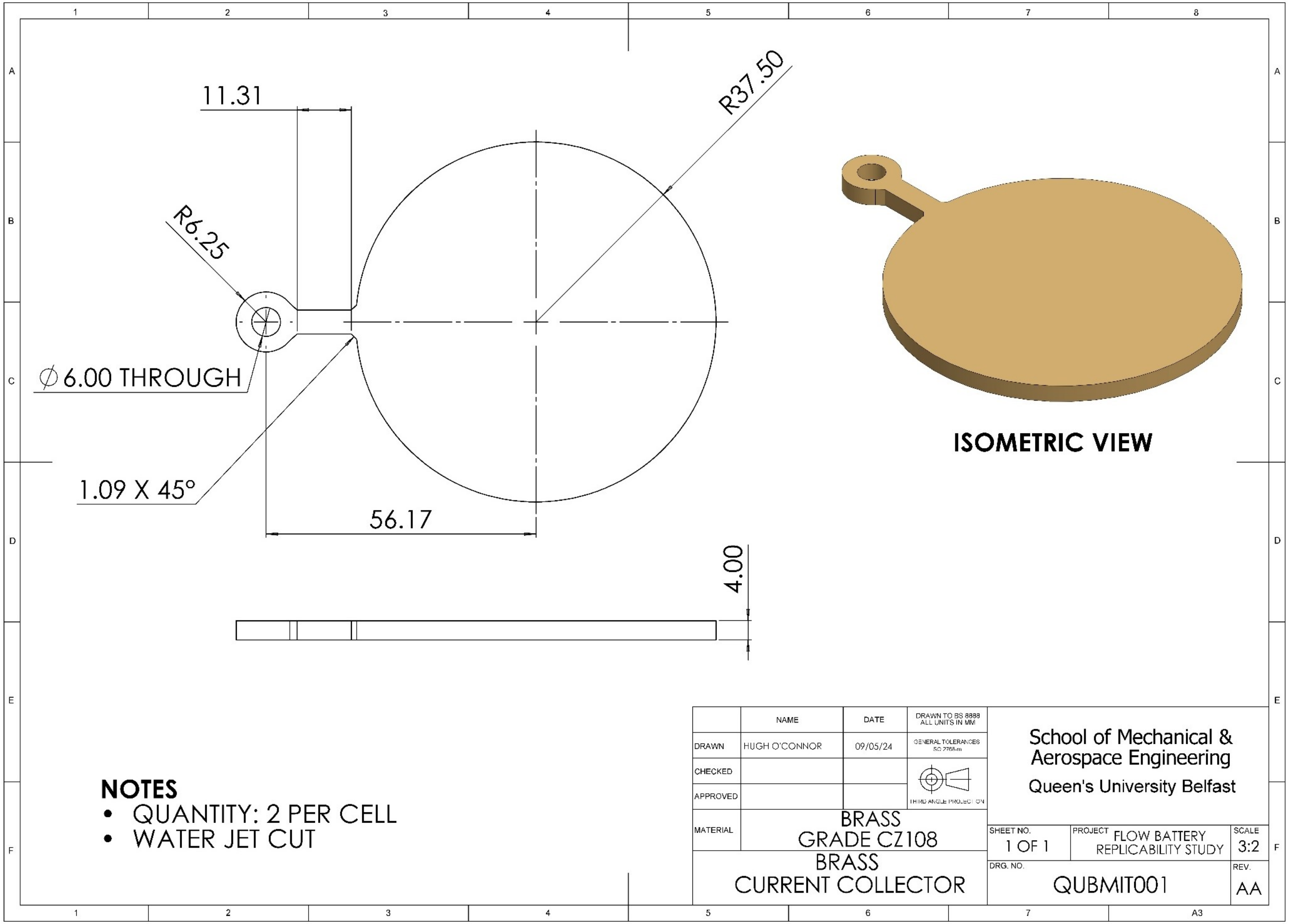

Figure S2. (**a**) Engineering drawing of brass current collector.

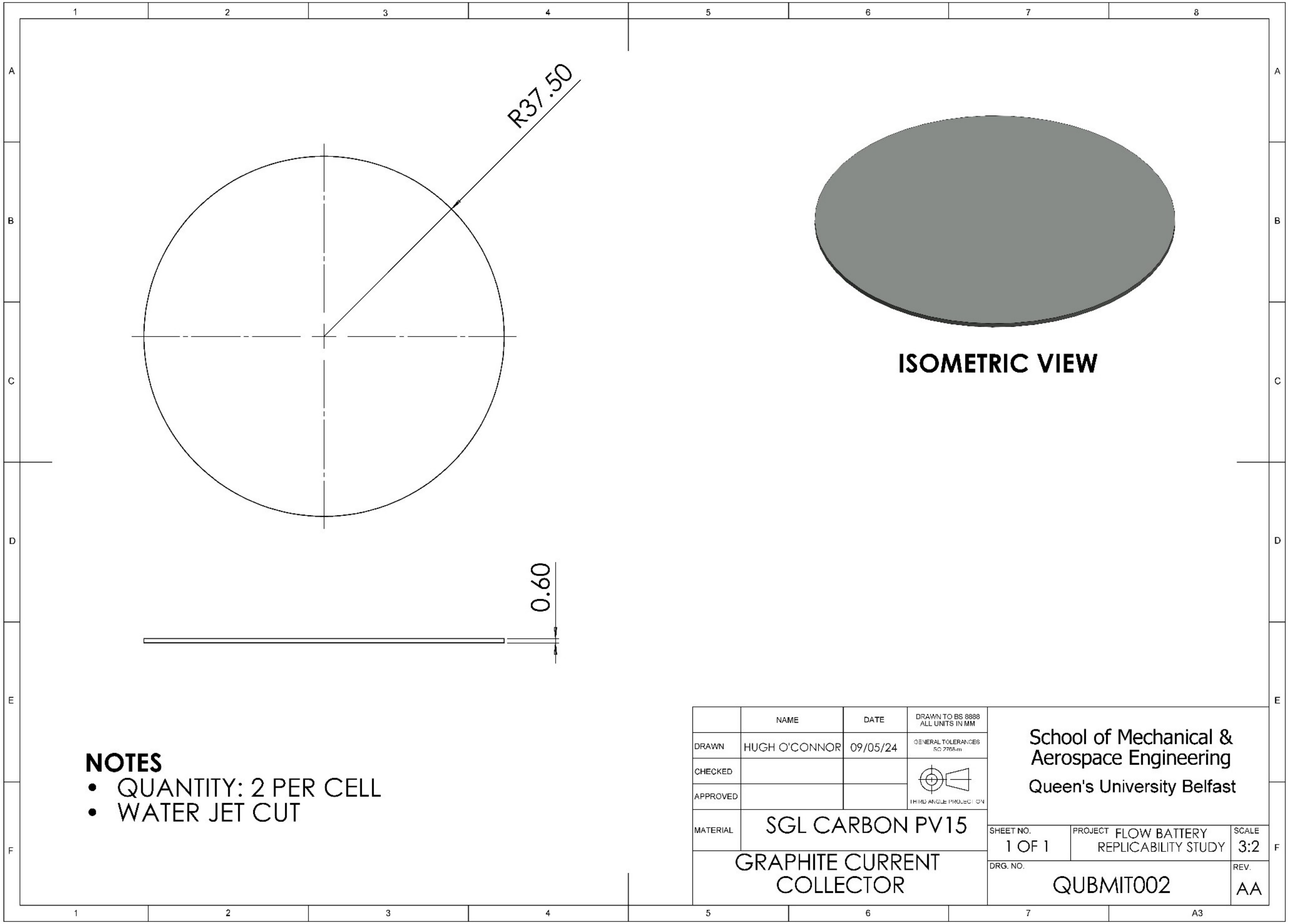

Figure S2. (**b**) Engineering drawing of graphite current collector

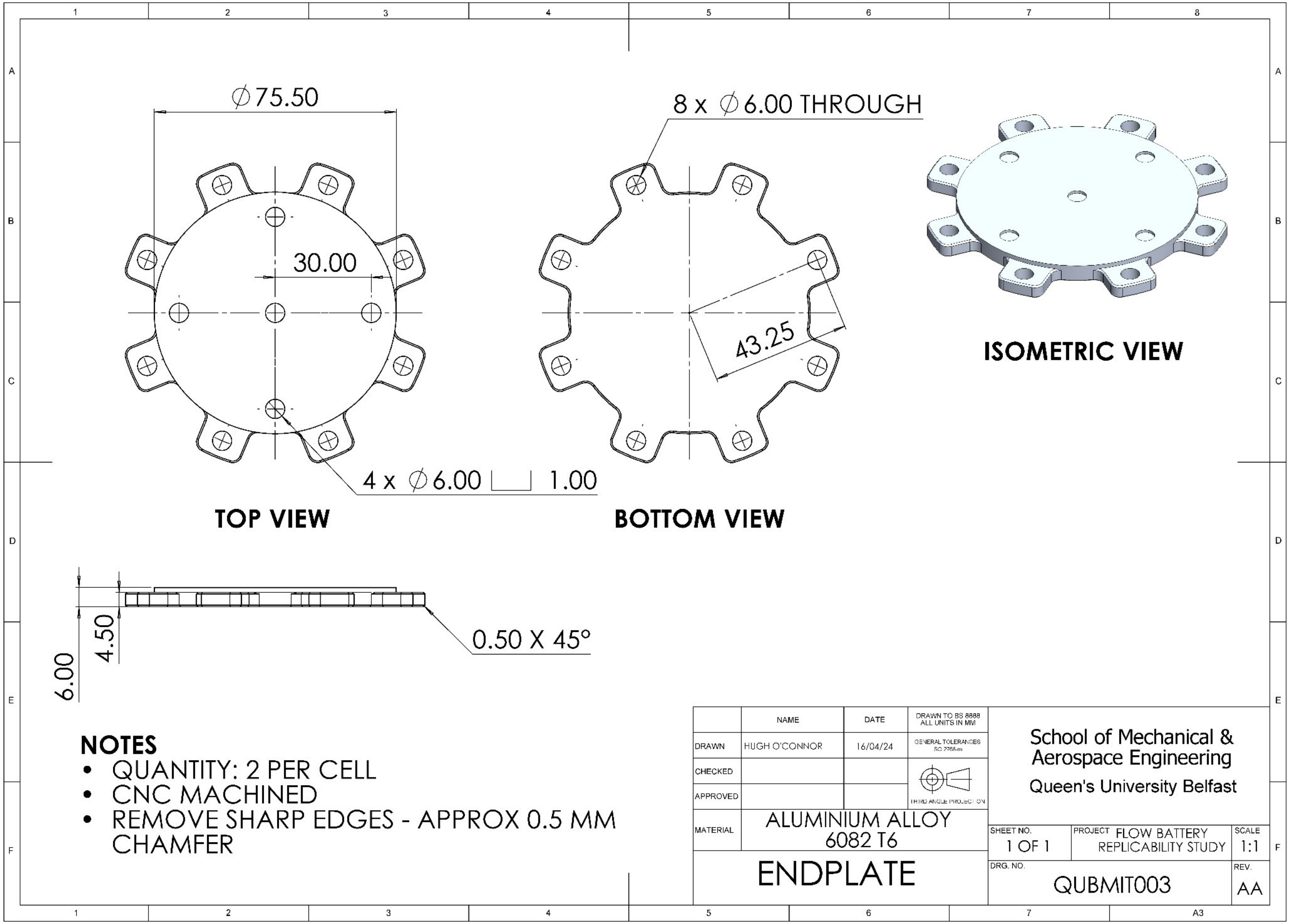

NOTES
- QUANTITY: 2 PER CELL
- CNC MACHINED
- REMOVE SHARP EDGES - APPROX 0.5 MM CHAMFER

	NAME	DATE	DRAWN TO BS 8888 ALL UNITS IN MM
DRAWN	HUGH O'CONNOR	16/04/24	GENERAL TOLERANCES ISO 2768-m
CHECKED			
APPROVED			THIRD ANGLE PROJECTION
MATERIAL	ALUMINIUM ALLOY 6082 T6		

ENDPLATE

School of Mechanical &
Aerospace Engineering
Queen's University Belfast

SHEET NO. 1 OF 1
PROJECT FLOW BATTERY REPLICABILITY STUDY
SCALE 1:1
DRG. NO. QUBMIT003
REV. AA

Figure S2. (**c**) Engineering drawing of aluminium endplate

Section S2: Additional data collection and analysis notes

Theoretical capacity

The theoretical capacity (Q_t) is calculated by **Equation S1**, where n is the number of electrons transferred *per* molecule of active species converted (here, $n = 1$), C (mol L^{-1}) is the concentration of the dissolved active species, V (L) is the electrolyte volume in a single reservoir, F is Faraday's constant (96485 C mol^{-1}), and 3.6 is a conversion factor (C mAh^{-1}).

$$Q_t = nCVF/3.6 \tag{S1}$$

For 100 mL of electrolyte containing 100 mM potassium ferricyanide, 100 mM potassium ferrocyanide, the theoretical capacity is *ca.* 536 mAh.

Additional impedance fitting details

The transfer function for the equivalent circuit model used to fit the data is given by **Equation S2**, where Z (Ω) is the impedance of the flow cell, j is the unit imaginary number, ω (s^{-1}) the frequency of the voltage (or current) sinusoid, L (H) is the inductance of the electrical leads, R_Ω (Ω) the combined ohmic resistance of the membrane and other ionic/electronic conducting components, R_{CT} (Ω) the charge transfer resistance at the electrode-electrolyte interface, W_δ (Ω) the finite-length Warburg element, and Z_{CPE} (Ω) the constant phase element (CPE).

$$Z = j\omega L + R_\Omega + \left(\frac{1}{Z_{CPE}} + \frac{1}{R_{CT} + W_\delta}\right)^{-1} \tag{S2}$$

Equation S3 expands the CPE into the variables j, ω, γ (-), and Q (F s$^{\gamma-1}$).

$$Z_{CPE} = \frac{1}{(j\omega)^\gamma Q} \tag{S3}$$

Equation S4 expands the Warburg element into j, ω, a resistance term (R_d, Ω), and a timescale τ_d (s).

$$W_\delta = R_d \frac{tanh\sqrt{\tau_d j\omega}}{\sqrt{\tau_d j\omega}} \tag{S4}$$

In the Python code, the equivalent circuit is represented by the string 'R0-L0-p(R1-Ws1,CPE1)', where '-' separates circuit elements in series and 'p()' places comma-separated elements contained in the parentheses in parallel. The elements contained in this string are mapped to the variable names in this document as such: R0 = R_Ω, L0 = L, R1 = R_{CT}, Ws1 = W_δ, and CPE1 = Z_{CPE}. The input parameters are input by a vector with the following variables [R0, L0, R1, Ws1_0, Ws1_1, CPE1_0, CPE1_1], where Ws1_0 = R_d, Ws1_1 = τ_d, CPE1_0 = Q, CPE1_1 = γ. The initial guess for each parameter in the vector listed above (with the units mentioned above) is given by "initial_guess = [0.1,1e-7,0,0.1,1,1,1]". Parameters were constrained to be non-negative (i.e., > 0). An upper bound of 1 was assigned to the CPE1_1 = γ, reflecting limiting behaviour of an ideal capacitor. All other parameters were not constrained to any upper limit value. Excepted where stated below, all data was included in the fit. Some input values were further refined to achieve better fits.

Due to challenges in obtaining fits which visually aligned with the data, some data was excluded from the fit or the parameters further constrained, as mentioned here. For P2, frequencies above 5 × 10^4 Hz were cropped due to stray reactance and CPE1_0 was limited to an upper value of 10^{-2} due to pinning of the fit to the upper bound of 1. This modified upper bound was selected to be ca. an order of magnitude higher than that of the other fits. For P3b, P5, and P6b, frequencies above 5 × 10^4 Hz were cropped to minimize overrepresentation in the unweighted fit towards highly negative -Im(Z) values. Additionally, for P6b, the upper bound of CPE1_0 was limited to an upper value of 5 × 10^{-4} based on fits to similar spectra in the dataset which did not pin the CPE1_0 to 1.

The quality of the first were quantified by the relative residuals given by **Equation S5**.

$$residual = (Z - Z_{fit})/Z \tag{S5}$$

Except for P4 at 1 mL min^{-1}, all fits were within 5% residual for both the real and imaginary parts. Further information about the fitting routine, fit quality (including standard error estimates and residuals), and plots can be explored in the Jupyter Notebook contained in the "EISanalysis" folder within the **Supplemental File "Data and code.zip"**.

Recollected datasets

Five datasets, tagged with a "b" (P2b, P3b, P6b, P7b, P8b), were partially or fully re-collected due to a range of issues that fell beyond the remit of replicability error including active species precipitation (P2), incorrect electrolyte composition (P3, P6), a leak during charge-discharge cycling (P7), and a change to conditioning procedure due to low accessed capacity (electrolyte pumped overnight through the cell) in addition to performing the experiment in the ambient environment as opposed to inside a glovebox (P8). In the main text, we focus on the datasets free from these issues (P1, P2, P3b, P4, P5, P6b, P7, and P8b) for polarisation/impedance and (P1, P2b, P3b, P4, P5, P6b, P7b, and P8b) for cycling and correlations between charge-discharge (CD) cycling/impedance/polarisation. **Figures S3, S4,** and **S5** compare re-collected with original data. Polarisation data (**Figure S3**) is largely the same for P2/P2b, whereas new polarisation data (P3b, P6b, and P8b) demonstrates better performance than prior polarisation data from the same respective participants (P3, P6, and P8). The same conclusions are drawn from impedance (**Figure S4**), with the exception of P3/P3b. P3b, while seemingly having a smaller arc, has a higher x-axis intercept, suggesting a larger ohmic resistance. For all re-collected cycling data (**Figure S5**), the newer results exhibited higher capacity.

In the main text, polarisation and impedance data from P2 were reported due to comparable data at 10, 30, and 50 mL min^{-1} (data at these flow rates are compared in **Figure S6**). Except for CD cycling, P2b data (only collected at 50 mL min^{-1}) is similar to that collected in P2. P2 impedance and polarisation is compared to P2b cycling data in the correlations (**Figure S7**).

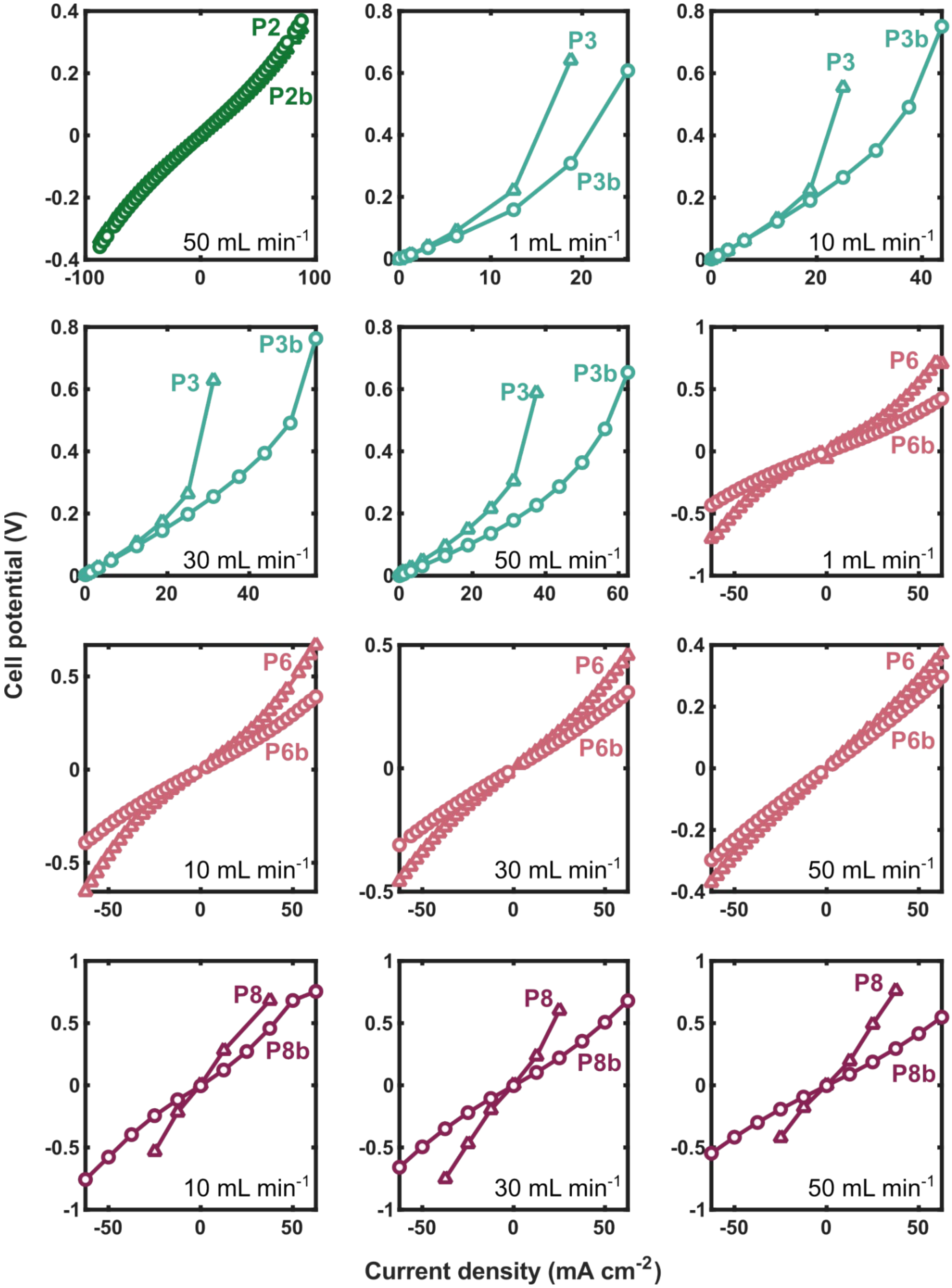

Figure S3. Comparison between the original and re-collected polarisation data for the subset of participants who re-collected data. In all cases, the re-collected data is denoted with “b”.

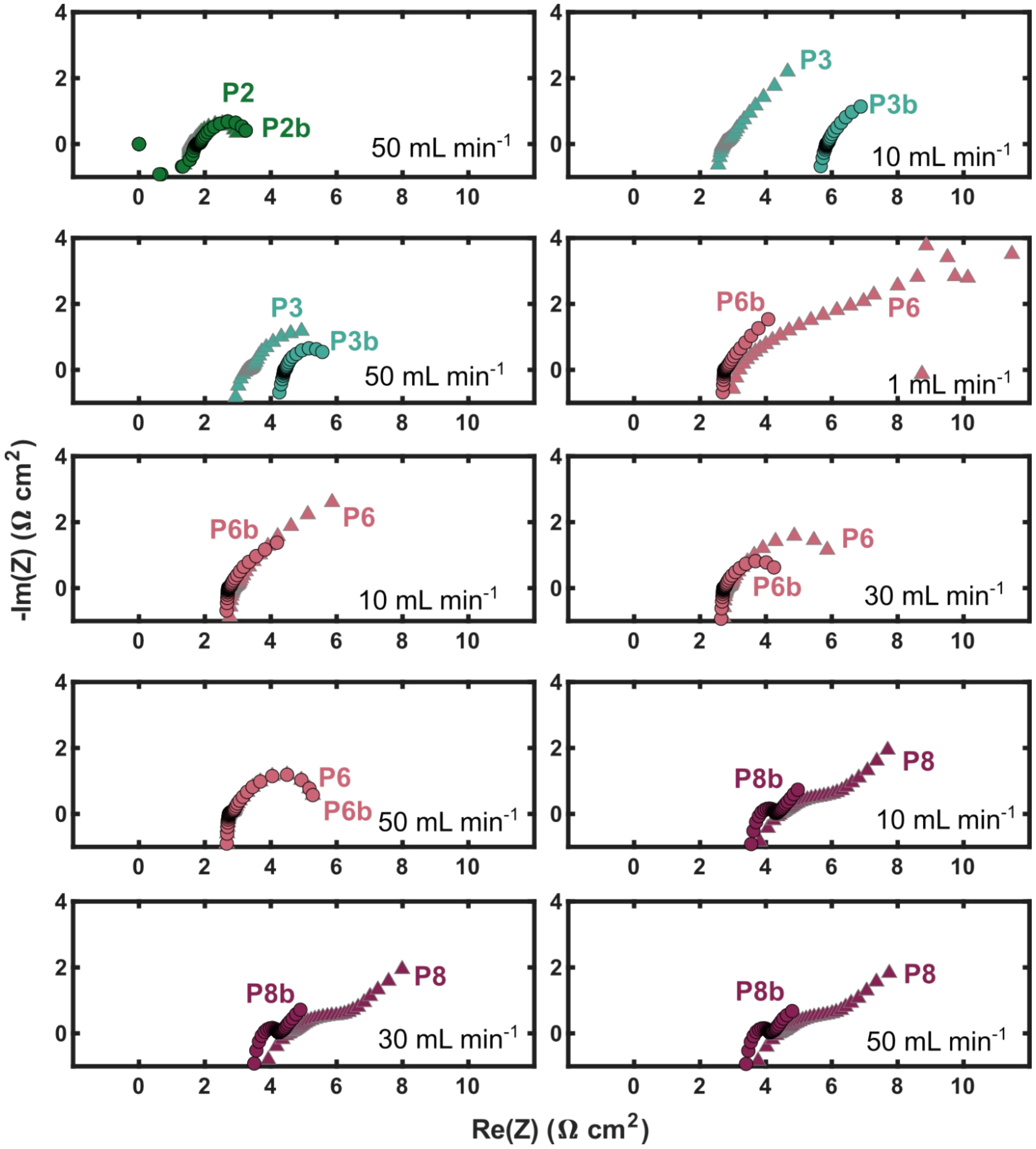

Figure S4. Nyquist plots comparing the original and re-collected data for the subset of participants who re-collected data. In all cases, the re-collected data is denoted with "b".

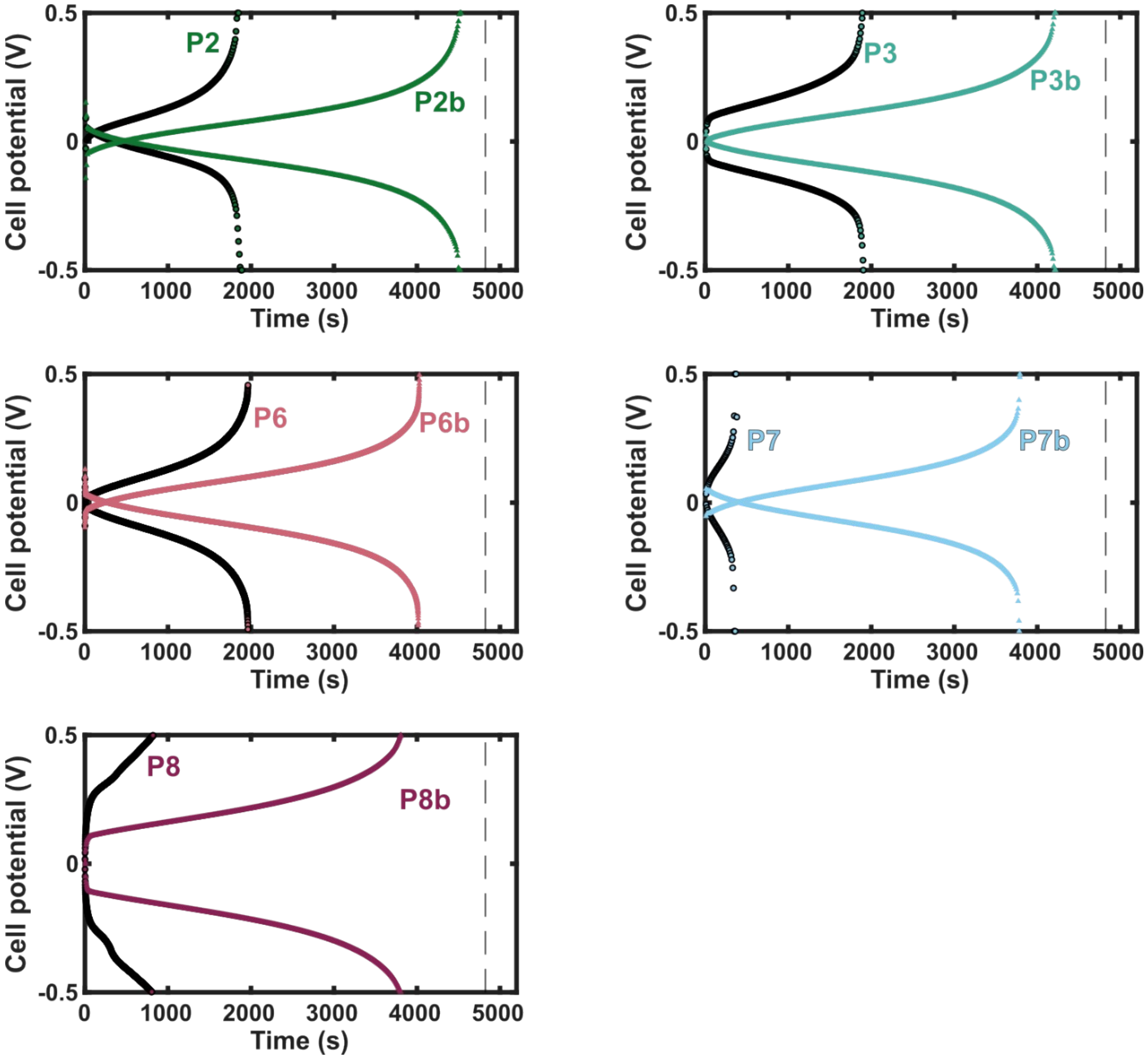

Figure S5. Comparison between the original and re-collected charge-discharge-cycling data (cycle 10) for the subset of participants who re-collected data. In all cases, the re-collected data is denoted with “b”. The grey vertical dashed line in all plots represented the theoretical charge/discharge time for the cell (derived from the theoretical capacity and constant current).

Pre-request flow cell testing

Prior to requesting experiments and data from the participants, the study leads sought to ensure that the experimental parameters were accessible using the same cell in two different laboratories (including some distinct auxiliary equipment), such that the flow cell system of interest was somewhat repeatable. Additionally, we explored variable reservoir volume sizes, settling on 100 mL as a compromise between minimizing material use (lower electrolyte volumes) with minimizing SoC drift (higher electrolyte volumes). In **Figure S6**, impedance, polarization and cycling capacity for charge-discharge are shown for these preliminary tests. Note that this data is collected under greater specification than ask of the participants, to avoid disagreement due to uncontrolled experimentation. However, even in this case, while excellent agreement is observed for the polarisation, there is some disagreement in the impedance shapes (mainly in the “kinetic” and “mass transport” arcs) and disagreement in the charge-discharge capacity accessed (Cell 2 exceeds that of Cell 1 by 6%).

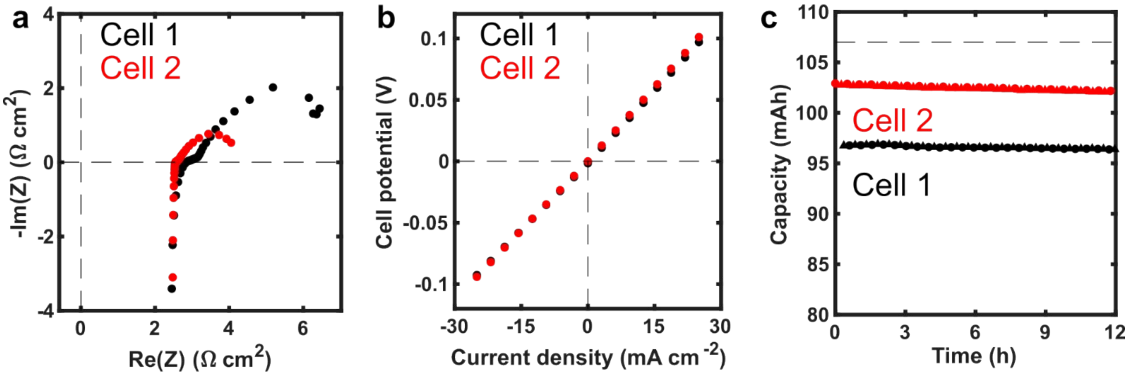

Figure S6. (a) Nyquist plot, (b) polarisation curves, and (c) charge-discharge cycling capacities collected by AHQ and HOC prior to sending experimental request to participants at their respective institutions. Panels are presented in order of data collection. Data here was collected using all of the same parameters as described in the main text except that 20 mL volumes of electrolyte were used instead of 100 mL. Flow rate was set to 50 mL min^{-1} for the three experiments. Polarisation was collected at the following sequence of current densities [0, 3.13, -3.13, 6.25, -6.25, 9.38, -9.38, 12.5, -2.5, 15.6, -15.6, 18.8, -18.8, 21.9, -21.9, 25, -25] mA cm^{-2} with 30 s duration per polarization step. Impedance was collected at 10 mV root-mean-square amplitude, 6 points log-spaced *per* decade between 200 kHz and 10 mHz with 3 measurements averaged *per* frequency. CD cycling data was collected at 25 mA cm^{-2}. The dashed grey line in (c) represents the theoretical capacity of the cell.

Differences in participants' set-ups

Differences in the choices *per* participant are compiled in **Tables S3-S5**. **Table S3** shows variations in reservoir material/geometry, application of stirring/sparging, electrode preparation, and electrical connections, **Table S4** shows contrasts in electrochemical protocol for impedance and polarisation, and **Table S5** shows additional dissimilarities in flow cell operation. These tables serve to illustrate typical choices made by researchers in this study. However, they do not easily explain or correlate with flow cell performance and we caution against drawing conclusions due to the many disparities in set-up choices, history and state-dependent effects of the electrolyte and electrode (*e.g.*, due to experimental ordering), environmental differences (*e.g.*, temperature, exposure of electrolyte to light), and further unaccounted-for factors.

Table S3. A summary of as-reported experimental details for individual participants, including reservoir material, the method used to measure electrolyte volume, whether or not stirring was employed in the reservoirs, whether or not sparging was employed in the reservoirs, the volume of electrolyte prepared from which 100 mL was sampled for each reservoir, the tool(s) used to cut electrodes, the electrical connector type, and whether 2- or 4- probe measurements were used. Here, PEIS is potentiostatic electrochemical impedance spectroscopy, pol is polarisation, and CD is charge-discharge cycling.

	Reservoir material	**Electrolyte volume measurement**	**Electrolyte stirring**	**Electrolyte sparging**	**Batch volume (mL)**	**Electrode cutting**	**Electrical connector**	**2- or 4-probe measurement**
P1	Glass	Graduated cylinder	No	No	500	Hard cardboard template, razor blade	Crocodile clips	4 for PEIS & pol, 2 for CD
P2b	Glass	Graduated cylinder	Yes	20 min with dry Ar	250	Razor blade	Crocodile clips	4
P3b	Glass	Graduated cylinder	No	No	1000	Razor blade	Brass screws	2
P4	Glass	Volumetric flask	No	No	250	Scissors	Crocodile clips	2
P5	Glass	Graduated cylinder	No	Humid N_2	100	Razor blade	Banana plugs	2
P6b	Glass	Volumetric flask	Yes	Humid N_2	1000	Stainless steel die	Crocodile clips	4
P7	Glass	Syringe	No	Dry "inert gas"	250	Scalpel	Crocodile clips	2
P8b	PP	Graduated cylinder	No	No	200	Razor blade	Crocodile clips	2

Table S4. A summary of as-reported electrochemical testing parameters for individual participants, including the duration of the polarisation step, the potential or current interval between steps, the maximum current measured during polarisation, whether galvanostatic (GEIS) or potentiostatic (PEIS) electrochemical impedance spectroscopy was used, and the peak-to-peak or root-mean square amplitude (RMS) of the impedance signal, where reported.

	Polarisation pulse length (s)	**Polarisation intervals**	**Max. current (mA)**	**EIS type**	**EIS amplitude (peak-to-peak)**
P1	30	50 mV	2800	PEIS	10 mV (RMS)
P2b	30	50 mA	1400	GEIS	Unreported
P3b	120	10, 50, or 100 mA	640	PEIS	10 mV
P4	120	100 mA	1000	PEIS	5 mV
P5	90	100 mA	2000	PEIS	10 mV
P6b	30	50 mA	1000	PEIS	10 mV (RMS)
P7	30	100 mA	500	PEIS	Unreported
P8b	60	200 mA	1000	PEIS	10 mV (RMS)

Table S5. A summary of as-reported operational details for the individual participants, including a measurement of the average laboratory temperature (T_{avg}) near the flow cell during the experiment, whether componentry was replaced, whether the cell was conditioned, if and how the pump was calibrated, as well as the order of the electrochemical techniques applied (where "EIS" is electrochemical impedance spectroscopy, "pol" is polarisation, and "CD" is charge-discharge cycling), and other notes (*e.g.*, issues encountered during data collection).

	T_{avg} (°C)	Replaced components	Cell conditioning	Pump calibration	Order of tests	Other notes
P1	21.0	Electrolyte replaced after polarisation	Pumped electrolytes for 25 min	Water, graduated cylinder, with cell	EIS, pol, CD	1.6 mL excess volume in one tank
P2b	21.0	None	Pumped electrolytes for 20 min, inverted cell many times to remove trapped gas	Water, graduated cylinder, with cell	EIS, pol (50 mL/min only), CD	
P3b	21.5	Fresh electrolyte for each polarisation	Pumped electrolytes for 10 min	Yes - manual measurement	EIS, pol, CD	
P4	21.0	Gaskets, electrolyte and electrodes halfway through CD	Pumped electrolytes for 30 min	No	EIS, pol, CD (1 mL/min EIS, pol at end)	Volume reduced to 80 mL after 4 days - some crystallisation around tubing in lid. Bottom of cell had a small crack + black deposits on brass current collector.
P5	23.3	None	Pumped electrolytes for 20 min, repeated POL and EIS at 50 mL/min	Water, graduated cylinder, with cell	EIS, pol, CD	Tube burst at end of life
P6b	18.8	None	Pumped electrolyte for 3 h	Water, graduated cylinder, with cell	Just repeated CD	
P7	22.0	None	Pumped electrolytes for 30 min	Water, graduated cylinder, with cell	pol, EIS, CD	A leak from reservoirs before cycling began - leaving a low capacity, slightly lower capacities at night, possibly due to temperature variation.
P8b	24.5	None	Pumped electrolyte overnight at 100 mL/min	Water, graduated cylinder, without cell	For each flow rate, EIS + pol, then CD	

Figure S6 contains polarisation curves that span the entire current density and potential range of the data collected by all participants at all reported flow rates. These plots highlight the differences in selected ranges, and choices to either polarize the cell positively or positively and negatively. As such, we opted to show the data only from 0 - 60 mA cm^{-2} in the main text.

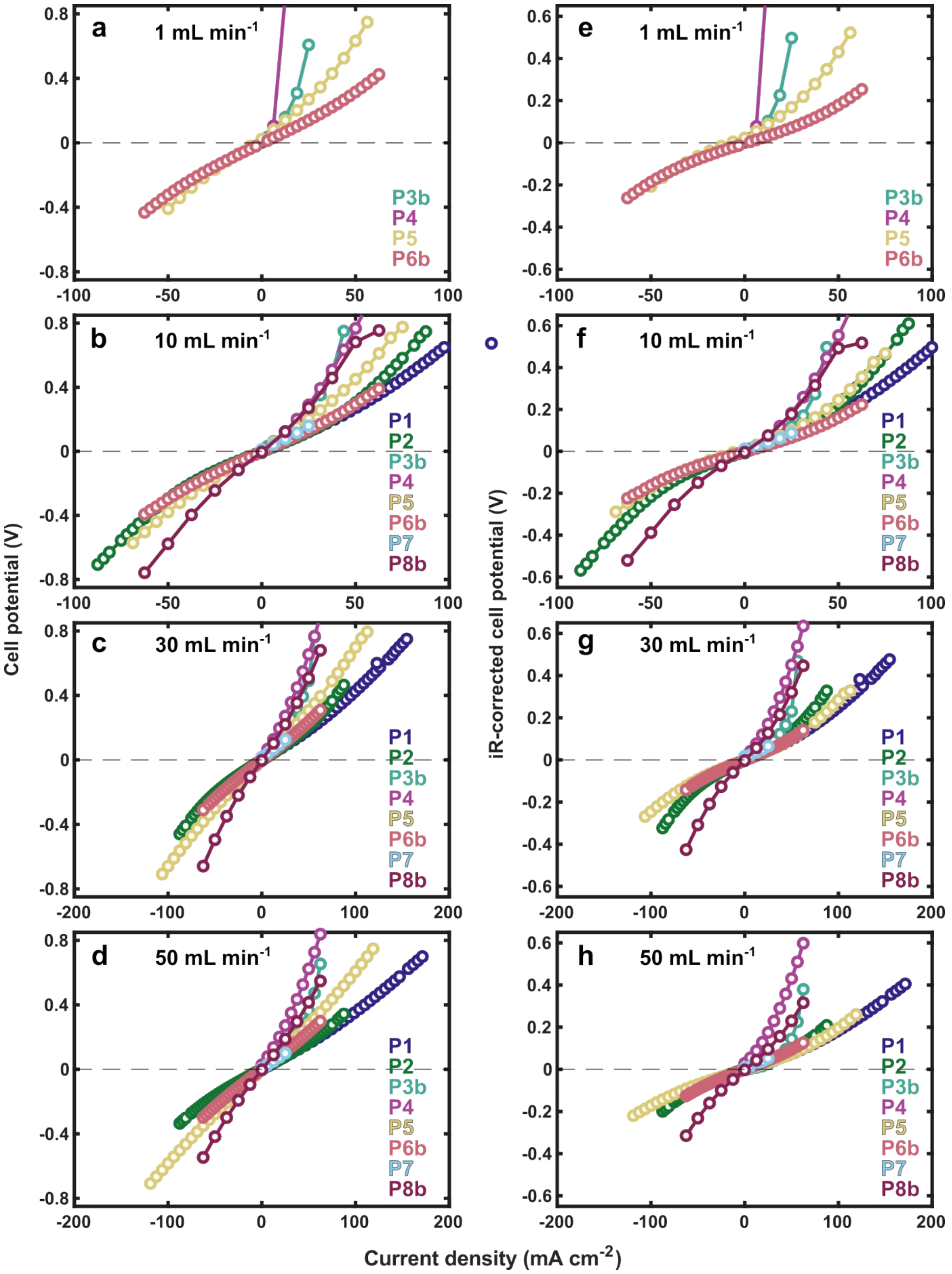

Figure S7. Polarisation at all flow rates tested, for positive and negative polarisation, and for all spanning current densities and potentials collected. Cell polarisation measurements without iR correction at (a) 1 mL min^{-1}, (b) 10 mL min^{-1}, (c) 30 mL min^{-1}, and (d) 50 mL min^{-1}. iR-corrected cell polarisation at (e) 1 mL min^{-1}, (f) 10 mL min^{-1}, (g) 30 mL min^{-1}, and (h) 50 mL min-^{1}. The current and potential for the last 10 seconds of each step were averaged to yield each point.

Figure S8 a-c contains the mean cell potential (E_{mean}), the standard deviation in cell potential (σ), and the corresponding coefficient of variation (σ/E_{mean}) for data between -60 to 60 mA cm^{-2}, for all studied flow rates (1, 10, 30, and 50 mL min^{-1}). Further, the number of data points (N) used to calculate the mean/standard deviation/coefficient of variation, which changes with current density due to the participants providing data across distinct ranges, is plotted in **Figure S8 d**. iR-corrected cell potential as well as its corresponding standard deviation and coefficient of variation are also provided in **Figure S8 e-h**. Note that **Figure S8 d** is identical to **Figure S8 h**, but is shown again, aligned with the x-axes of **Figure S8 e-f**, to facilitate comparison.

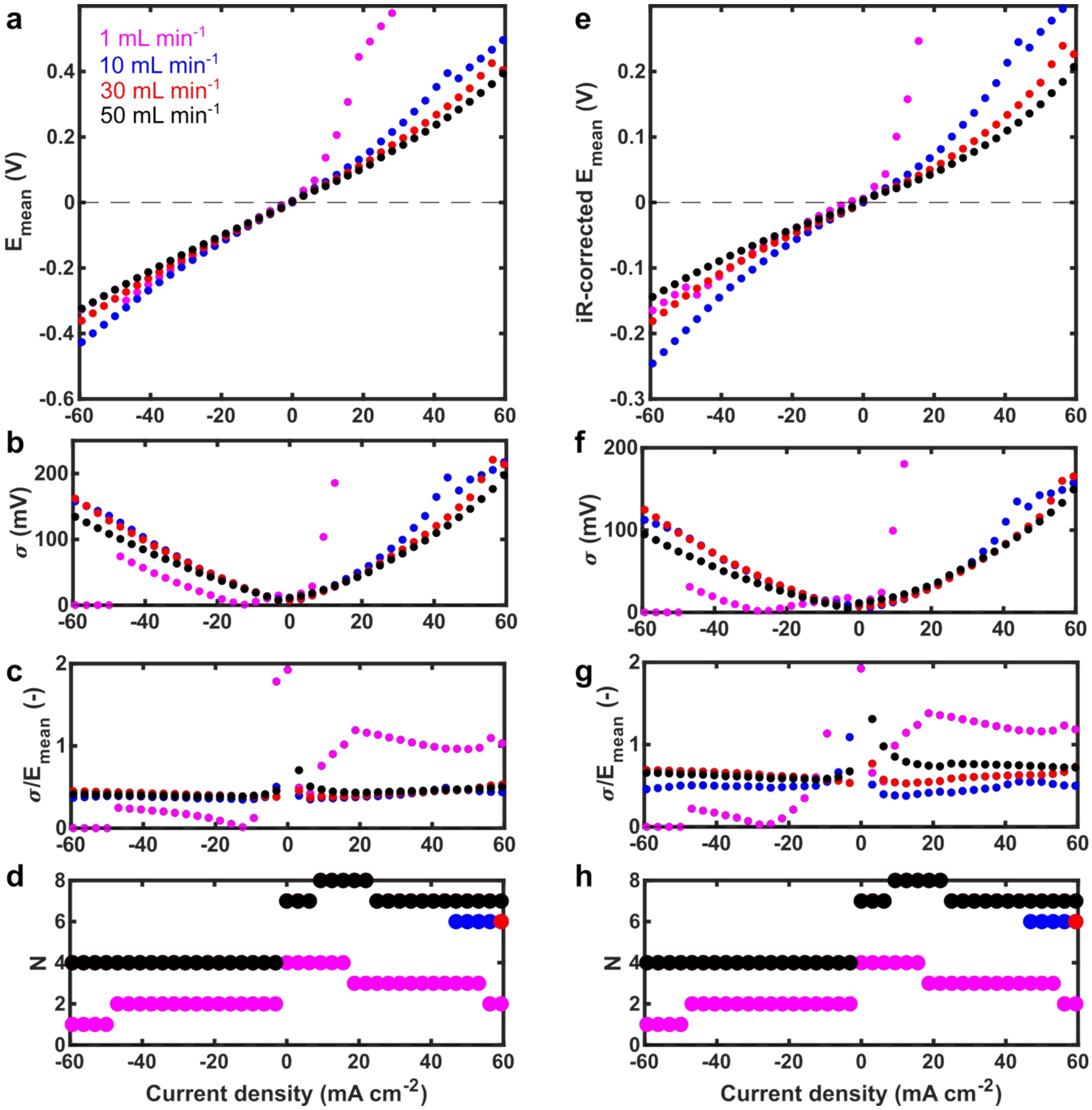

Figure S8. Comparison of (a) polarisation curve with mean cell potential across all participants calculated at each current density, (b) standard deviation about the mean cell potential, and (c) coefficient of variation at 1, 10, 30, and 50 mL min^{-1} over a current density range of -60 to 60 mA cm^{-2} (d) Number of participant's data contributing to each data point. (e-h) same as (a-d) but for iR-corrected polarisation data. (d) is equivalent to (h). In both (d) and (h), some dots overlap each other in the order of top to bottom: black, red, blue, magenta. The current and potential for the last 10 seconds of each step were averaged to yield each point.

Additional impedance data at 1 mL min^{-1}

Figure S9 shows impedance data at 1 mL min^{-1}. This is reported here, as opposed to the main text, due to the majority of participants (5/8) lacking the capability to set this low flow rate using the same configuration for data collected at the other flow rates. With the exception of P4, the high-frequency features of the impedance (*i.e.*, the x-axis intercept and the size of the first arc, attributed to reaction kinetics) are roughly the same as those observed in **Figure 5**. The mass transport arc, due to the lower flow rates, would require lower frequency measurements to better observe. As such, we refrain on commenting on the trend of this arc. P4 seemingly has a kinetic arc twice the size than observed at 10, 30, and 50 mL min^{-1} suggesting electrode behaviour that improves during or after collecting polarisation and EIS data at 1 mL min^{-1}.

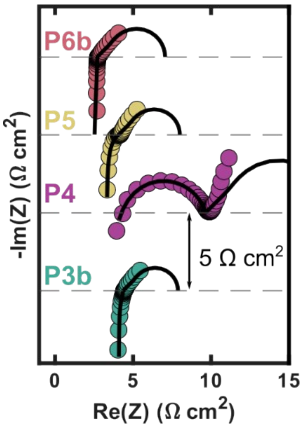

Figure S9. Nyquist plots of flow cells at 1 mL min^{-1} flow rate collected by a subset of participants.

Pairwise metric correlations

Figure S10 and **S11** provide two scatterplots for each pair of ASR$_{pol}$ (Ω cm^2), ASR$_{pol,iR\text{-}corr}$ (Ω cm^2), ASR$_{EIS}$ (Ω cm^2), R_{Ω} (Ω cm^2), R_{CT} (Ω cm^2), R_{MT} (Ω cm^2), ASR$_{EIS,iR\text{-}corr}$ (R_{CT} + R_{MT}, Ω cm^2), electrolyte utilisation (EU, %), coulombic efficiency (CE, %), discharge voltage averaged across all 19 charge-discharge cycles (V_{dch}, V), charge voltage averaged across all 19 charge-discharge cycles (V_{ch}, V), and decay rate (% day^{-1}). **Figure S10** contains all data, whereas **Figures S11** focuses on the dataset for polarisation excluding P3b, P4, P7, and P8b. Beyond the correlations described in the main text (**Figure 10**, ASR$_{EIS}$/ASR$_{pol}$, ASR/V$_{dch,}$ and ASR$_{pol}$/EU), **Figure S10** highlights some degree of correlation for the following pairs of quantities: V_{ch}/V_{dch}, ASR$_{pol,iR\text{-}corr}$/ASR$_{EIS,iR\text{-}corr}$, ASR$_{pol,iR\text{-}corr}$/R_{MT}, ASR$_{pol,iR\text{-}corr}$/R_{CT}, ASR$_{EIS,iR\text{-}corr}$/R_{CT}, and ASR$_{EIS,iR\text{-}corr}$/R_{CT}. The correlation of V_{ch}/V_{dch} is expected due to the symmetric flow cell configuration and identical electrolyte in both reservoirs, and thus nominally identical charge-discharge behaviour. Interestingly, correlations involving R_{CT}/R_{MT}/ASR$_{pol,iR\text{-}corr}$/ASR$_{EIS,iR\text{-}corr}$ are less-pronounced when excluding P3b, P4, P7, and P8b (due to the issues identified the main text: positive polarisation, outlier behaviour, compromised current collector) while other correlations strengthen (those of iR- and non-iR-corrected ASR$_{pol}$/ASR$_{EIS}$ and R_{Ω}) as shown in **Figures S11**. This suggests that for the excluded group, ohmic losses explain most of the variations whereas the roles of R_{MT} and R_{CT} are increasingly important for the outliers. V$_{ch}$ (or V$_{dch}$) correlate more strongly in this group with ASR$_{pol,iR\text{-}corr}$, ASR$_{EIS,iR\text{-}corr}$, and R$_{\Omega}$, suggesting better inter-technique agreement. CE/EU also correlate more-strongly, although this group include “P1” and thus should be interpreted cautiously. Otherwise, weak or no correlations are observed between EU and CE and the other variables. While these correlations coarsely suggest the importance of ohmic losses and potentially R_{MT} and R_{CT} for some cells, the small number of samples might lead to some coincidental correlations.

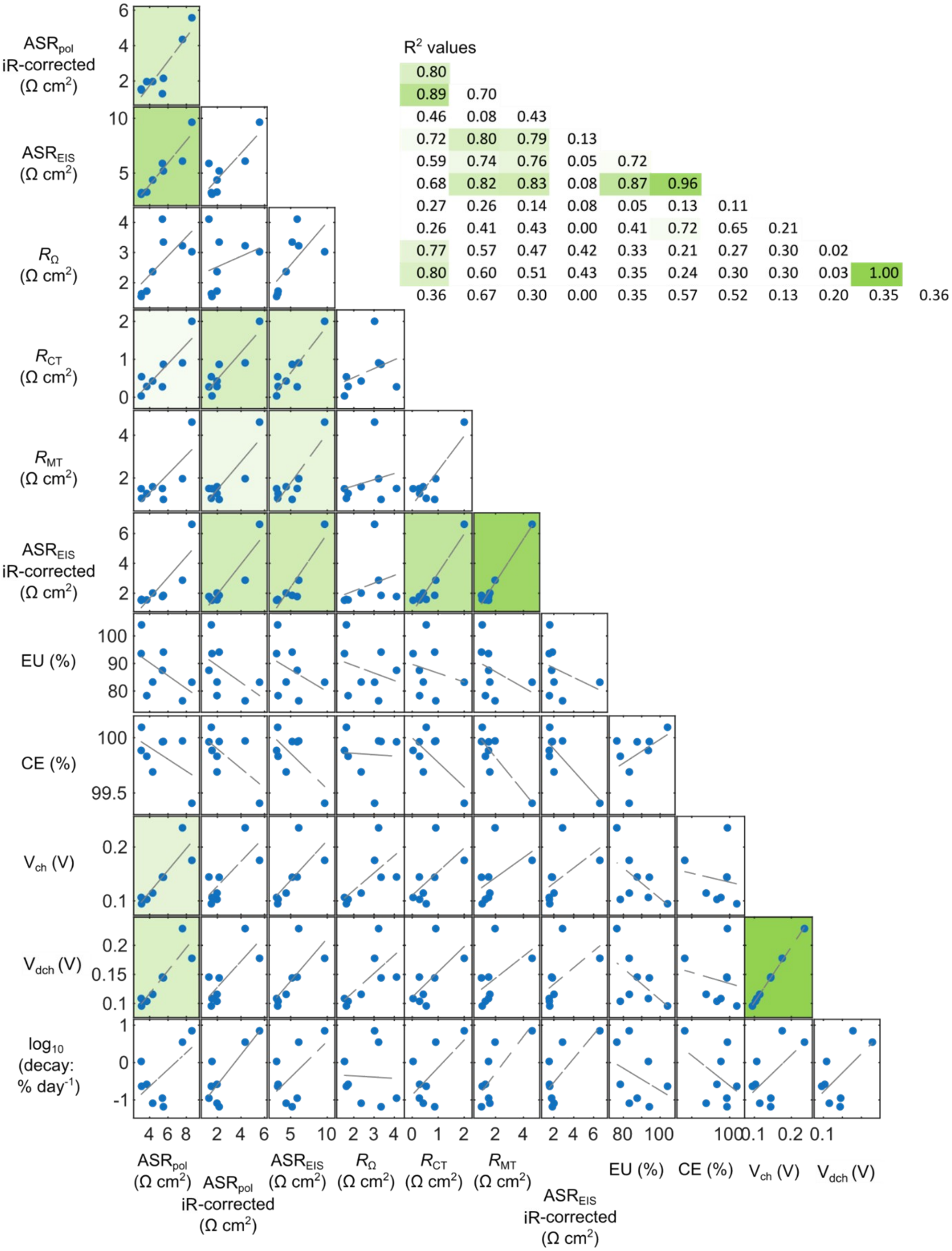

R^2 values

0.80										
0.89	0.70									
0.46	0.08	0.43								
0.72	0.80	0.79	0.13							
0.59	0.74	0.76	0.05	0.72						
0.68	0.82	0.83	0.08	0.87	0.96					
0.27	0.26	0.14	0.08	0.05	0.13	0.11				
0.26	0.41	0.43	0.00	0.41	0.72	0.65	0.21			
0.77	0.57	0.47	0.42	0.33	0.21	0.27	0.30	0.02		
0.80	0.60	0.51	0.43	0.35	0.24	0.30	0.30	0.03	1.00	
0.36	0.67	0.30	0.00	0.35	0.57	0.52	0.13	0.20	0.35	0.36

Figure S10. Pairwise correlation scatterplot for all data to highlight relationships between performance metrics collected across polarisation, impedance, and CD cycling. Dashed lines are regression lines fit by the ordinary least squares method. The coefficient of determination (R^2) value for each linear fit is the number shown in the top right of the figure.

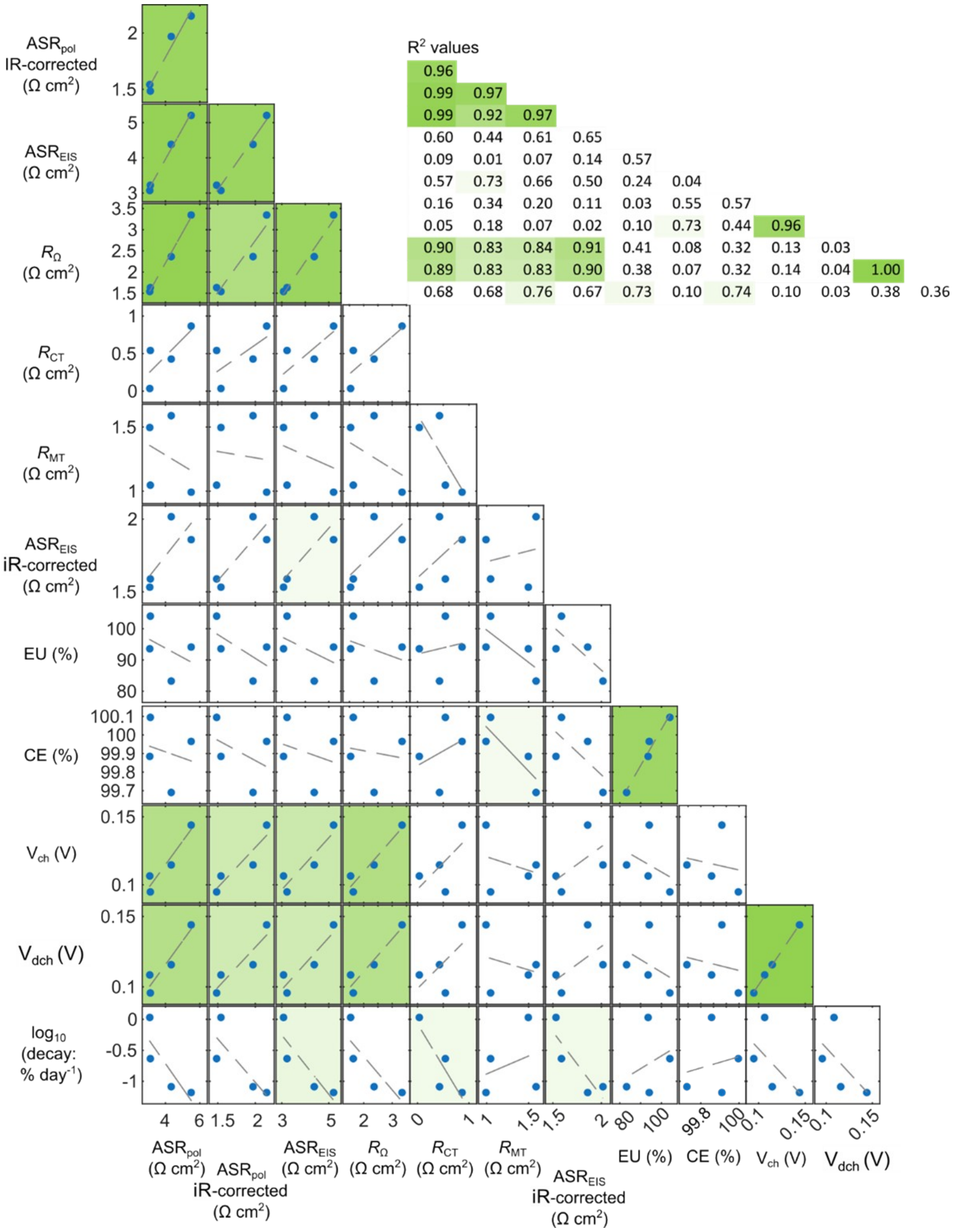

0.96										
0.99	0.97									
0.99	0.92	0.97								
0.60	0.44	0.61	0.65							
0.09	0.01	0.07	0.14	0.57						
0.57	0.73	0.66	0.50	0.24	0.04					
0.16	0.34	0.20	0.11	0.03	0.55	0.57				
0.05	0.18	0.07	0.02	0.10	0.73	0.44	0.96			
0.90	0.83	0.84	0.91	0.41	0.08	0.32	0.13	0.03		
0.89	0.83	0.83	0.90	0.38	0.07	0.32	0.14	0.04	1.00	
0.68	0.68	0.76	0.67	0.73	0.10	0.74	0.10	0.03	0.38	0.36

Figure S11. Pairwise correlation scatterplot for the dataset excluding P3b, P4, P7, and P8b (the same dataset for the polarization curves of **Figure 4**) to highlight relationships between performance metrics collected across polarisation, impedance, and CD cycling. Dashed lines are regression lines fit by the ordinary least squares method. The coefficient of determination (R^2) value for each linear fit is the number shown in the top right of the figure.

In **Table S6**, we include statistics measures for metrics explored in the main text for all participants, excluding P3b, P4, P7, and P8b (as done so for polarisation analysis, meant to highlight correlations between ASRs and polarisation/EIS metrics), and excluding P1, P4b, and P8b (for cycling metrics reported in **Table 1,** generally meant to highlight the spread in EU).

Table S6. Statistics across metrics for various groups of participants.

	Mean	Std	IQR	Q75	Q25		Median
All participants							
$\mathrm{ASR_{pol}}$	5.161	2.042	3.136	6.537	3.402	4.861	5.161
$\mathrm{ASR_{EIS}}$	5.099	2.196	2.745	5.994	3.249	4.793	5.099
$\mathrm{R_{\Omega}}$	2.621	0.948	1.608	3.285	1.677	2.695	2.621
$\mathrm{R_{CT}}$	0.668	0.615	0.606	0.887	0.281	0.484	0.668
$\mathrm{R_{MT}}$	1.810	1.176	0.619	1.778	1.159	1.501	1.810
$\mathrm{ASR_{pol,iR\text{-}corr}}$	2.540	1.559	1.739	3.252	1.513	1.967	2.540
$\mathrm{ASR_{EIS,iR\text{-}corr}}$	2.478	1.729	0.873	2.445	1.572	1.820	2.478
EU (%)	87.565	9.233	13.106	93.868	80.762	85.391	87.565
CE (%)	99.851	0.215	0.207	99.968	99.761	99.924	99.851
V_{ch} (V)	0.140	0.047	0.055	0.160	0.105	0.129	0.140
V_{dch} (V)	0.140	0.045	0.055	0.162	0.106	0.130	0.140
Decay (% day^{-1})	-1.555	2.525	2.202	-0.097	-2.299	-0.247	-1.555
Excluding P3b, P4, P7, P8b							
$\mathrm{ASR_{pol}}$	4.008	1.151	1.815	4.915	3.101	3.726	4.008
$\mathrm{ASR_{EIS}}$	3.970	1.010	1.645	4.793	3.148	1.755	3.970
$\mathrm{R_{\Omega}}$	2.221	0.835	1.268	2.855	1.588	3.801	2.221
$\mathrm{R_{CT}}$	0.468	0.343	0.473	0.704	0.231	1.999	0.468
$\mathrm{R_{MT}}$	1.281	0.305	0.523	1.543	1.020	0.484	1.281
$\mathrm{ASR_{pol,iR\text{-}corr}}$	1.787	0.325	0.547	2.060	1.513	1.272	1.787
$\mathrm{ASR_{EIS,iR\text{-}corr}}$	1.749	0.228	0.377	1.937	1.560	1.723	1.749
EU (%)	93.756	8.480	10.653	99.083	88.429	93.868	93.756
CE (%)	99.909	0.169	0.242	100.030	99.788	99.925	99.909
V_{ch} (V)	0.115	0.021	0.029	0.129	0.101	0.111	0.115
V_{dch} (V)	0.116	0.020	0.028	0.130	0.102	0.112	0.116
Decay (% day^{-1})	-0.363	0.479	0.579	-0.074	-0.652	-0.157	-0.363
Excluding P1, P4b, P8b							
$\mathrm{ASR_{pol}}$	4.398	1.053	1.882	5.416	3.535	4.333	4.398
$\mathrm{ASR_{EIS}}$	4.365	1.213	2.151	5.376	3.225	4.381	4.365
$\mathrm{R_{\Omega}}$	2.616	1.093	1.861	3.537	1.676	2.365	2.616
$\mathrm{R_{CT}}$	0.378	0.307	0.321	0.537	0.216	0.285	0.378
$\mathrm{R_{MT}}$	1.371	0.242	0.325	1.526	1.201	1.497	1.371
$\mathrm{ASR_{pol,iR\text{-}corr}}$	1.781	0.358	0.538	2.015	1.477	1.964	1.781
$\mathrm{ASR_{EIS,iR\text{-}corr}}$	1.749	0.206	0.349	1.898	1.549	1.782	1.749
EU (%)	87.370	6.766	11.700	93.732	82.031	87.518	87.370
CE (%)	99.867	0.113	0.167	99.963	99.797	99.885	99.867
V_{ch} (V)	0.122	0.020	0.038	0.144	0.106	0.115	0.122
V_{dch} (V)	0.123	0.020	0.037	0.144	0.107	0.116	0.123
Decay (% day^{-1})	-0.319	0.429	0.387	-0.078	-0.464	-0.112	-0.319

References

1 H. O'Connor, J. J. Bailey, O. M. Istrate, P. A. A. Klusener, R. Watson, S. Glover, F. Iacoviello, D. J. L. Brett, P. R. Shearing and P. Nockemann, *Sustainable Energy Fuels*, 2022, **6**, 1529–1540.